

Boyu MA, Zongwu XIE, Zainan JIANG, Hong LIU

# Precise semi-analytical inverse kinematic solution for 7-DOF offset manipulator with arm angle optimization

© The Author(s) 2021. This article is published with open access at link.springer.com and journal.hep.com.cn

**Abstract** Seven-degree-of-freedom redundant manipulators with link offset have many advantages, including obvious geometric significance and suitability for configuration control. Their configuration is similar to that of the experimental module manipulator (EMM) in the Chinese Space Station Remote Manipulator System. However, finding the analytical solution of an EMM on the basis of arm angle parameterization is difficult. This study proposes a high-precision, semi-analytical inverse method for EMMs. Firstly, the analytical inverse kinematic solution is established based on joint angle parameterization. Secondly, the analytical inverse kinematic solution for a non-offset spherical-roll-spherical (SRS) redundant manipulator is derived based on arm angle parameterization. The approximate solution of the EMM is calculated in accordance with the relationship between the joint angles of the EMM and the SRS manipulator. Thirdly, the error is corrected using a numerical method through the analytical inverse solution based on joint angle parameterization. After selecting the stride and termination condition, the precise inverse solution is computed for the EMM based on arm angle parameterization. Lastly, case solutions confirm that this method has high precision, and the arm angle parameterization method is superior to the joint angle parameterization method in terms of parameter selection.

**Keywords** 7-DOF redundant manipulator, inverse kinematics, semi-analytical, arm angle, link offset

## 1 Introduction

Space robots play an irreplaceable role in human space exploration [1–4]. The Space Station Remote Manipulator System (SSRMS) [5], special purpose dexterous manipulator [6], and European Robotic Arm [7] applied to the International Space Station [8] are all 7-degree-of-freedom (7-DOF) redundant manipulators. Space robots also include the Chinese Space Station Remote Manipulator System (CSSRMS) [9], TianGong-2 manipulator [10], Robonaut 2 [11], Japanese Experiment Module Remote Manipulator System [12], and ETS-VII manipulator [13]. CSSRMS consists of a core module manipulator (CMM) and an experimental module manipulator (EMM) [14], which are also 7-DOF redundant manipulators with link offset. The EMM can not only be mounted at the end of the CMM to perform precise operations but also operate independently. They work together to maintain CSSRMS. The kinematics of these manipulators is particularly important when they are performing given tasks. The manipulator discussed in this study is the EMM.

Seven-DOF redundant manipulators have more joint DOFs than the dimension of its operating space. When they perform given tasks, additional constraints, namely, obstacle avoidance [15,16], singularity handling [17,18], joint torque optimization [19,20], and fault-tolerant control [21–23], must be considered. However, the inverse kinematic solution of redundant manipulators is more difficult than that of non-redundant manipulators. The solution can be solved in the position domain [24] or velocity domain [25,26]. The precision of the position-domain solution is high, but multiple solutions need to be dealt with. The self-motion of manipulators can be controlled in the velocity domain by adopting the gradient projection method to optimize the given tasks [27,28]. However, the solution in the velocity domain produces several numerical errors. This study investigates the inverse kinematic solution of redundant manipulators in the position domain.

Seven-DOF redundant manipulators are classified into

Received October 10, 2020; accepted January 16, 2021

Boyu MA, Zongwu XIE, Zainan JIANG (✉), Hong LIU  
School of Mechatronics Engineering, Harbin Institute of Technology, Harbin 150001, China; State Key Laboratory of Robotics and System, Harbin Institute of Technology, Harbin 150001, China  
E-mail: jiangzainan@hit.edu.cn

two types: Non-offset spherical–roll–spherical (SRS) and offset manipulators. For convenience, offset manipulators are referred to as EMMs. The shoulder and wrist joints of the SRS manipulator have no offset, and its shoulder and wrist are spherical joints. The EMM has offsets at the shoulder and wrist joints. Therefore, its inverse solution is relatively complex. A few extant studies have examined the inverse kinematics of EMMs.

Focusing on the SRS manipulator, Lee and Bejczy [29] proposed a method to solve the analytical inverse kinematic solution for redundant manipulators on the basis of joint angle parameterization, but the selection of joint parameters in this method is difficult. Zu et al. [30] proposed a quadratic calculation method based on the errors caused by the gradient projection method and the accuracy of the joint angle parameterization method. This method reaches the given trajectory and improves the precision of the end-effector. Kreutz-Delgado et al. [31] presented the concept of arm angle. The geometric significance of the arm angle parameterization method is more obvious than that of the joint angle parameterization method. The former is suitable for configuration control of redundant manipulators. However, this method has two algorithm singularities, namely, the reference plane and the arm plane are not unique. The elbows of the SRS manipulator and the EMM in this work have offsets; hence, the second singularity does not exist. Shimizu et al. [32] solved the inverse kinematics of the SRS manipulator via arm angle parameterization and reported that this method is suitable for joint limits. Xu et al. [33] proposed the dual arm angle to avoid the singularity that arises when the reference plane is not unique and derived the absolute reference attitude matrix of the elbow. Solving the inverse kinematics of the SRS manipulator on the basis of arm angle parameterization is more convenient. Zhou et al. [34] presented a method for the inverse kinematics of the SRS manipulator with joint and attitude limits. In accordance with the arm angle range corresponding to the restriction of each joint, they obtained the arm angle range of the manipulator and selected the best arm angle. Then, the inverse kinematics of the manipulator was solved in the position domain. Dereli and Koker [35] proposed a swarm optimization method called firefly algorithm to solve the inverse kinematics of redundant manipulators. Other methods can be found in Refs. [36–38]. However, the previous method based on arm angle parameterization is only suitable for the SRS manipulator.

Focusing on the EMM, Crane et al. [39] proposed an inverse kinematic solution method based on spatial polygon projection. A 6-DOF subchain can be formed by parameterizing the value of joint angles  $\theta_1$ ,  $\theta_2$ , or  $\theta_7$ . By projecting it in space, eight solutions can be solved. This method is inconvenient because it involves the complex geometry of space. Yu et al. [40] presented a method using a virtual spherical wrist to replace the real offset wrist of a redundant manipulator with an offset wrist and assumed that

the two wrists have the same joint angle. The attitude of the end-effector of the manipulator with a spherical wrist was calculated by using that of the manipulator with an offset wrist. Then, the inverse kinematics solution of the manipulator with a spherical wrist was solved. Simulations for a single target point and continuous trajectory verified this method. Abbasi et al. [41] used the arm angle rate as an additional task constraint and controlled SSRMS by adopting the augmented Jacobian method. Lu et al. [42] proposed a method in which the orientation matrices and arm angle do not need to change during the movement of a redundant manipulator with link offset. The method is based on damped least-squares, and the inverse kinematic solution is solved by iterative calculation in the velocity domain. This method was verified through a simulation in which the end-effector tracked a circle with a constant orientation and arm angle. Jin et al. [43] proposed an optimization algorithm for determining the optimal elbow orientation on the basis of particle swarm optimization and solved the inverse kinematics by using the relationship between elbow orientation and joint angles. Xu et al. [44] solved the inverse kinematic solution of the SRS manipulator through arm angle parameterization and generalized the results to the EMM (referred to as the SSRMS manipulator in their paper) in accordance with the relationship of joint angles between the EMM and the SRS manipulator. However, the inverse kinematic solution for the EMM was approximate based on arm angle parameterization. The arm angles of the eight solutions had uncontrollable errors.

The geometric significance of the arm angle parameterization method is obvious, and it is suitable for configuration control and obstacle avoidance. The precise analytical solution cannot be solved based on arm angle parameterization because of the particularity of the configuration for the EMM, but an approximate solution was solved in Ref. [44]. No previous study has presented a method to solve the precise solution for the EMM on the basis of arm angle parameterization. The current study proposes a high-precision, semi-analytical inverse solution method for the EMM. We define nominal arm angle  $\psi$  and actual arm angle  $\tilde{\psi}$ . The approximate solution based on arm angle parameterization is corrected by the analytical solution based on joint angle parameterization. Then, the precise solution is solved. The superiority of the arm angle parameterization method in parameter selection is verified using cases. The studied cases prove that this method has high precision.

This paper is organized in the following manner. In Section 2, we establish a model of the EMM and provide the analytical inverse kinematic solution based on joint angle parameterization. In Section 3, the approximate analytical inverse kinematic solution for the EMM is derived based on arm angle parameterization. In Section 4, the approximate solution is corrected by a numerical method, and the high precision of this method is verified by cases. In Section 5, the superiority of the arm

angle parameterization method over the joint angle parameterization method in terms of parameter selection is analyzed.

## 2 Analytical solution based on joint angle parameterization

### 2.1 Kinematics modeling of the EMM

The configuration of the EMM used in this study is (R–Y–P)–P–(P–Y–R).  $a_i$  ( $i = 0, 1, \dots, 8$ ) is the link length of the EMM. The axes of joints 3, 4, and 5 are parallel. Shoulder offset  $a_1$  and wrist offset  $a_7$  are not zero. The D–H frame [45] is shown in Fig. 1(a). The initial configuration of the EMM is shown in Fig. 1(b). The D–H parameters are listed in Table 1.  $\Sigma_i$  ( $i = 0, 1, \dots, 7, EE$ ) ( $EE$  corresponds to end coordinate system  $\Sigma_{EE}$ ) is the coordinate system of this manipulator. The axes of base coordinate system  $\Sigma_0$  and end coordinate system  $\Sigma_{EE}$  are parallel to that of

the hand-eye-camera coordinate systems at the beginning and end of this manipulator, respectively.

### 2.2 Analytical solution of each joint angle

Define  $\theta_i$  ( $i = 1, 2, \dots, 7$ ) as the joint angle of the EMM. The homogeneous transformation matrix between the adjacent link coordinate systems of the manipulator is

$${}^{i-1}T_i = \begin{bmatrix} \cos\theta_i & -\sin\theta_i & 0 & a_{i-1} \\ \sin\theta_i \cos\alpha_{i-1} & \cos\theta_i \cos\alpha_{i-1} & -\sin\alpha_{i-1} & -d_i \sin\alpha_{i-1} \\ \sin\theta_i \sin\alpha_{i-1} & \cos\theta_i \sin\alpha_{i-1} & \cos\alpha_{i-1} & d_i \cos\alpha_{i-1} \\ 0 & 0 & 0 & 1 \end{bmatrix}. \quad (1)$$

For convenience of expression, we define  $c_i = \cos\theta_i$  and  $s_i = \sin\theta_i$ .

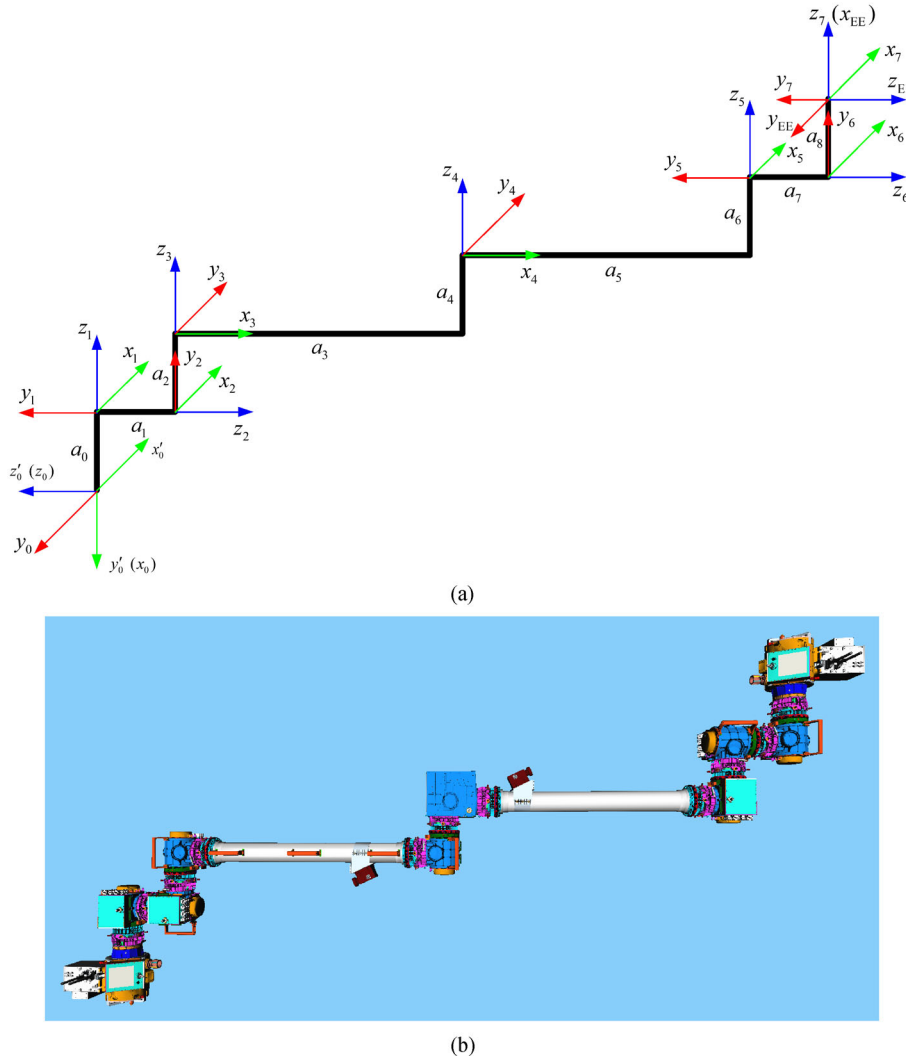


Fig. 1 Experimental module manipulator: (a) D–H frame and (b) initial configuration.

**Table 1** D–H parameters of the experimental module manipulator

Link $i$	$a_{i-1(\text{DH})}/\text{m}$	$\alpha_{i-1(\text{DH})}/(^{\circ})$	$d_{i(\text{DH})}/\text{m}$	$\theta_{i(\text{DH})}/(^{\circ})$
1	0	90	$a_0$	0
2	0	90	$a_1$	0
3	0	–90	$a_2$	–90
4	$a_3$	0	$a_4$	0
5	$a_5$	0	$a_6$	90
6	0	90	$a_7$	0
7	0	–90	$a_8$	0
8	0	90	0	90

Note:  $a_{i-1(\text{DH})}$  is the length of link, which is defined as the distance from  $z_{i-1}$  to  $z_i$  measured along  $x_{i-1}$  positive direction;  $\alpha_{i-1(\text{DH})}$  is the torsion angle of link, which is defined as the angle from  $z_{i-1}$  to  $z_i$  measured about  $x_{i-1}$  positive direction;  $d_{i(\text{DH})}$  is the offset distance of link, which is defined as the distance from  $x_{i-1}$  to  $x_i$  measured along  $z_i$  positive direction; and  $\theta_{i(\text{DH})}$  is the rotation angle of link, which is defined as the angle from  $x_{i-1}$  to  $x_i$  measured about  $z_i$  positive direction. Link 1 is relative to coordinate system  $\Sigma'_0$ , and link 8 is relative to coordinate system  $\Sigma_7$ .

The forward kinematic equation of the manipulator is

$${}^0T_{EE} = {}^0T_{0'} {}^0T_1 {}^1T_2 {}^2T_3 {}^3T_4 {}^4T_5 {}^5T_6 {}^6T_7 {}^7T_{EE}. \quad (2)$$

The homogeneous transformation matrix of end coordinate system  $\Sigma_{EE}$  relative to base coordinate system  $\Sigma_0$  is

$${}^0T_{EE} = \begin{bmatrix} n_x & s_x & a_x & p_x \\ n_y & s_y & a_y & p_y \\ n_z & s_z & a_z & p_z \\ 0 & 0 & 0 & 1 \end{bmatrix}, \quad (3)$$

where  $[n_x \ n_y \ n_z]^T$ ,  $[s_x \ s_y \ s_z]^T$ , and  $[a_x \ a_y \ a_z]^T$  are unit vectors represented by end coordinate system  $\Sigma_{EE}$  in base coordinate system  $\Sigma_0$ , and  $[p_x \ p_y \ p_z]^T$  is the position of the origin of end coordinate system  $\Sigma_{EE}$  in base coordinate system  $\Sigma_0$ .

Given the value of  $\theta_1$ , the analytical inverse kinematic solutions based on joint angle parameterization are as follows.

$\theta_2$  has two solutions, namely,

$$\theta_2 = \arcsin \frac{-(a_2 + a_4 + a_6)}{\sqrt{a^2 + b^2}} - \phi, \quad (4)$$

$$\theta_2 = \pi - \arcsin \frac{-(a_2 + a_4 + a_6)}{\sqrt{a^2 + b^2}} - \phi, \quad (5)$$

where  $a = a_0 + p_x - a_8 n_x$ ,  $b = (a_8 n_y - p_y) c_1 + (p_z - a_8 n_z) s_1$ , and  $\phi = \arctan 2(a, b)$ .

$\theta_6$  has two solutions, namely,

$$\theta_6 = \pm \arccos [-(n_z s_1 - n_y c_1) s_2 - n_x c_2]. \quad (6)$$

$\theta_7$  has only one solution, which is

$\theta_7 =$

$$\arctan 2 \left( -\frac{(a_z s_1 - a_y c_1) s_2 + a_x c_2}{s_6}, \frac{(s_z s_1 - s_y c_1) s_2 + s_x c_2}{s_6} \right).$$

(7)

When  $s_6 = 0$ , the axes of joints 5 and 7 are parallel, and the manipulator is in a singular configuration. Equation (7) cannot solve  $\theta_7$ . We have to solve it by  $s_6 = 0$  and  $c_6 = \pm 1$ . Then,  $\theta_7$  can take arbitrary values by solving it. Usually,  $\theta_7 = 0$ .

$\theta_4$  has two solutions, namely,

$$\theta_4 = \pm \arccos \frac{A^2 + B^2 - a_3^2 - a_5^2}{2a_3 a_5}, \quad (8)$$

where

$$A = a_7 [c_7 ((a_y c_1 - a_z s_1) c_2 + a_x s_2) + s_7 ((s_y c_1 - s_z s_1) c_2 + s_x s_2)] + a_8 [(n_y c_1 - n_z s_1) c_2 + n_x s_2] + (p_z s_1 - p_y c_1) c_2 - (p_x + a_0) s_2,$$

$$B = -a_1 + a_7 [(a_y s_1 + a_z c_1) c_7 + (s_y s_1 + s_z c_1) s_7] + a_8 (n_y s_1 + n_z c_1) - p_y s_1 - p_z c_1.$$

$\theta_3$  has only one solution, which is

$$\theta_3 = \arctan 2 [A(a_3 + a_5 c_4) - B a_5 s_4, B(a_3 + a_5 c_4) + A a_5 s_4]. \quad (9)$$

$\theta_5$  has only one solution, namely,

$$c_{345} = -[(s_z c_1 + s_y s_1) s_7 + (a_z c_1 + a_y s_1) c_7]. \quad (10)$$

When  $s_6 \neq 0$ ,

$$s_{345} = -\frac{n_z c_1 + n_y s_1}{s_6}, \quad (11)$$

$$\begin{aligned} \theta_5 &= (\theta_3 + \theta_4 + \theta_5) - (\theta_3 + \theta_4) \\ &= \arctan 2(s_{345}, c_{345}) - (\theta_3 + \theta_4), \end{aligned} \quad (12)$$

where  $c_{345} = \cos(\theta_3 + \theta_4 + \theta_5)$ ,  $s_{345} = \sin(\theta_3 + \theta_4 + \theta_5)$ ,

and  $\theta_{345} = \theta_3 + \theta_4 + \theta_5$ .

When  $s_6 = 0$ ,  $(\theta_3 + \theta_4 + \theta_5)$  can be solved in accordance with  $\theta_7 = 0$ .

In summary, when  $\theta_1$  or  $\theta_2$  is given, we can solve each joint angle of the manipulator in accordance with  ${}^0T_{EE}$ . Eight solutions are available.

### 3 Approximate analytical solution based on arm angle parameterization

The analytical solution cannot be solved based on arm angle parameterization because of the particularity of the configuration for the EMM. We can solve the analytical solution of the SRS manipulator with the same end position and attitude based on arm angle parameterization and generalize the results to the EMM in accordance with the relationship of joint angles between the EMM and the SRS manipulator. However, these results are approximate, and the errors are uncontrollable.

#### 3.1 Definition of arm angle and arm plane

Shoulder point  $S$  is the intersection point of the rotation axes of joints 1 and 2, elbow point  $E$  is the origin of coordinate system  $\Sigma_4$ , and wrist point  $W$  is the intersection point of the rotation axes of joints 6 and 7. In other words,  $S$ ,  $E$ , and  $W$  are the origins of D-H coordinate systems  $\Sigma_1$ ,  $\Sigma_4$ , and  $\Sigma_6$ , respectively.  $e$  is the vector from  $S$  to  $E$ , and  $w$  is the vector from  $S$  to  $W$ . Vector  $V$  is a unit vector parallel to the rotation axis of joint 1, and it is defined as  ${}^0V = [-1 \ 0 \ 0]^T$ . Vector  $d$  is the projection of vector  $e$  on vector  $w$ . Vector  $p$  is perpendicular to  $w$  and passes through point  $E$  (defined as  $p = e - d$ ). Vector  $k$  is on the plane that contains vectors  $V$  and  $w$  and perpendicular to  $w$ .

The reference plane is the plane that contains vectors  $V$  and  $w$ . The arm plane is the plane that contains points  $S$ ,  $E$ , and  $W$ . Arm angle  $\psi$  is the angle at which the reference plane rotates around vector  $w$  to coincide with the arm plane, as shown in Fig. 2.

If the configuration of the manipulator is known, the arm angle at the current moment can be calculated. The calculation processes are as follows:

$$\begin{aligned} w &= {}^0SW = {}^0w \\ &= {}^0P_{EE} - [-a_0 \ 0 \ 0]^T - {}^0R_{EE} [a_8 \ 0 \ 0]^T, \end{aligned} \quad (13)$$

$$\begin{aligned} {}^0T_e &= {}^0T_{0'} {}^{0'}T_1 {}^1T_2 {}^2T_3 {}^3T_4 - {}^0T_{0'} {}^{0'}T_1 \\ &= \begin{bmatrix} * & * & * & e_x \\ * & * & * & e_y \\ * & * & * & e_z \\ 0 & 0 & 0 & 1 \end{bmatrix}, \end{aligned} \quad (14)$$

$$e = {}^0SE = {}^0e = [e_x \ e_y \ e_z]^T, \quad (15)$$

where  ${}^0P_{EE}$  and  ${}^0R_{EE}$  are the position vector and rotation matrix of end coordinate system  $\Sigma_{EE}$  in base coordinate system  $\Sigma_0$ , respectively,  ${}^0w$  and  ${}^0e$  are vectors expressed by  $w$  and  $e$  in base coordinate system  $\Sigma_0$ , respectively,  $*$  means that the calculation results are not listed.

The projection of vector  $e$  on vector  $w$  is

$$d = \hat{w}(\hat{w}^T e), \quad \hat{w} = \frac{w}{\|w\|}, \quad (16)$$

where  $\hat{w}$  is the unit vector of  $w$ ,  $\|\cdot\|$  denotes the norm of a vector.

The unit vector perpendicular to  $w$  on the arm plane is

$$\hat{p} = \frac{p}{\|p\|}, \quad p = e - d = (I_3 - \hat{w}\hat{w}^T)e, \quad (17)$$

where  $\hat{p}$  is the unit vector of  $p$ ,  $I_3$  is a  $3 \times 3$  identity matrix.

The unit vector perpendicular to  $w$  on the reference plane is

$$\hat{k} = \frac{k}{\|k\|}, \quad k = w \times (w \times V), \quad (18)$$

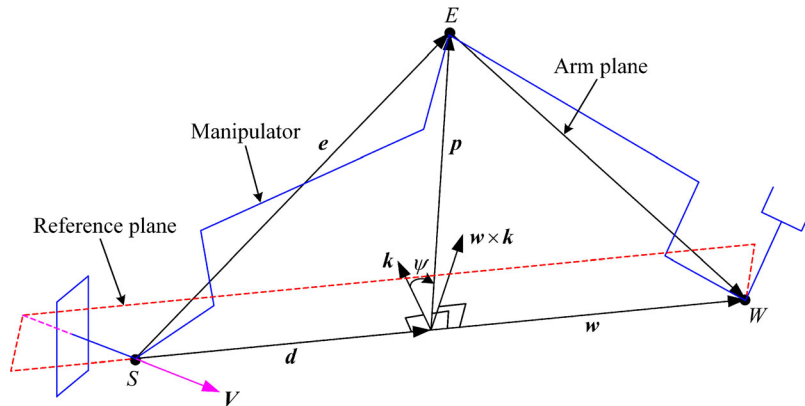


Fig. 2 Reference plane, arm plane, and arm angle of the experimental module manipulator.



expression of  ${}^0\mathbf{e}^0$  obtained from Fig. 3 is

$${}^0\mathbf{e}^0 = \frac{\mathbf{R}(\mathbf{l}, \alpha) \cdot {}^0\mathbf{w}^0}{\|{}^0\mathbf{w}^0\|} \|{}^0\mathbf{e}^0\|, \quad (25)$$

where  $\mathbf{l} = \mathbf{V} \times \mathbf{w}$ ,  $\|{}^0\mathbf{e}^0\|^2 = a_3^2 + (a_2 + a_4)^2$ , and  $\mathbf{R}(\mathbf{l}, \alpha) = \mathbf{I}_3 + [\mathbf{u}_l \times] \sin \alpha + [\mathbf{u}_l \times]^2 (1 - \cos \alpha)$ .  ${}^0\mathbf{w}^0$  and  ${}^0\mathbf{e}^0$  are vectors expressed by  ${}^0\mathbf{w}$  and  ${}^0\mathbf{e}$  when arm angle  $\psi = 0$ , respectively.  $\alpha$  is the angle from  ${}^0\mathbf{w}^0$  rotation to  ${}^0\mathbf{e}^0$ .  $[\mathbf{u}_l \times]$  denotes the skew-symmetric matrix of vector  $\mathbf{l}$ .

By using the cosine law for the triangle  $SEW$ , we obtain

$$a_5^2 + a_6^2 = \|{}^0\mathbf{e}^0\|^2 + \|{}^0\mathbf{w}^0\|^2 - 2\|{}^0\mathbf{e}^0\| \cdot \|{}^0\mathbf{w}^0\| \cos \alpha. \quad (26)$$

Referring to the configuration of the manipulator, we know that parameter  $\alpha \leq 90^\circ$ . Therefore,  $\alpha$  has only one solution, that is,

$$\alpha = \arccos \frac{\|{}^0\mathbf{e}^0\|^2 + \|{}^0\mathbf{w}^0\|^2 - a_5^2 - a_6^2}{2\|{}^0\mathbf{e}^0\| \cdot \|{}^0\mathbf{w}^0\|}. \quad (27)$$

These parameters are substituted into Eq. (25) to solve  ${}^0\mathbf{e}^0$ .

In accordance with Fig. 3, the expressions can be obtained as follows:

$$\begin{cases} a_6 {}^0\mathbf{z}_4^0 + a_5 {}^0\mathbf{x}_4^0 = {}^0\mathbf{w}^0 - {}^0\mathbf{e}^0, \\ (a_2 + a_4) {}^0\mathbf{z}_4^0 + a_3 {}^0\mathbf{x}_3^0 = {}^0\mathbf{e}^0, \end{cases} \quad (28)$$

where  ${}^0\mathbf{x}_4^0$ ,  ${}^0\mathbf{z}_4^0$ , and  ${}^0\mathbf{y}_4^0$  in the following derivation are unit vectors of three coordinate axes of coordinate system  $\Sigma_4$  relative to base coordinate system  $\Sigma_0$  when arm angle  $\psi = 0$ , and  ${}^0\mathbf{x}_3^0$  has the same meaning.

From the characteristic of the rotation matrix, we obtain

$$\begin{aligned} {}^4\mathbf{R}_3 = {}^3\mathbf{R}_4^{-1} &= \begin{bmatrix} c_{4'} & -s_{4'} & 0 \\ s_{4'} & c_{4'} & 0 \\ 0 & 0 & 1 \end{bmatrix}^{-1} \\ &= [{}^4\mathbf{x}_3 \quad {}^4\mathbf{y}_3 \quad {}^4\mathbf{z}_3], \end{aligned} \quad (29)$$

where  ${}^4\mathbf{x}_3$ ,  ${}^4\mathbf{y}_3$ , and  ${}^4\mathbf{z}_3$  are unit vectors of three coordinate axes of coordinate system  $\Sigma_3$  relative to coordinate system  $\Sigma_4$ .

Therefore,

$$\begin{aligned} {}^0\mathbf{x}_3^0 &= {}^0\mathbf{R}_4^{\psi=0} \cdot {}^4\mathbf{x}_3 = [{}^0\mathbf{x}_4^0 \quad {}^0\mathbf{y}_4^0 \quad {}^0\mathbf{z}_4^0] \begin{bmatrix} c_{4'} \\ -s_{4'} \\ 0 \end{bmatrix} \\ &= c_{4'} {}^0\mathbf{x}_4^0 - s_{4'} {}^0\mathbf{y}_4^0. \end{aligned} \quad (30)$$

${}^0\mathbf{x}_3^0$  is substituted into Eq. (28). Both sides of these equations are calculated by cross-multiplication. The new equation is simplified to

$$\begin{aligned} a_3 a_6 s_{4'} {}^0\mathbf{x}_4^0 + [a_3 a_6 c_{4'} - a_5 (a_2 + a_4)] {}^0\mathbf{y}_4^0 - a_3 a_5 s_{4'} {}^0\mathbf{z}_4^0 \\ = {}^0\mathbf{w}^0 \times {}^0\mathbf{e}^0. \end{aligned} \quad (31)$$

In accordance with Eqs. (28) and (31), we obtain

$$\begin{cases} {}^0\mathbf{x}_4^0 = \frac{a_3 a_6 s_{4'} ({}^0\mathbf{w}^0 \times {}^0\mathbf{e}^0) - a_5 a_5 s_{4'}^2 ({}^0\mathbf{e}^0 - {}^0\mathbf{w}^0)}{a_3^2 s_{4'}^2 (a_5^2 + a_6^2) + [a_5 (a_2 + a_4) - a_3 a_6 c_{4'}]^2} \\ \quad - \frac{[a_5 (a_2 + a_4) - a_3 a_6 c_{4'}] [a_6 {}^0\mathbf{e}^0 + (a_2 + a_4) ({}^0\mathbf{e}^0 - {}^0\mathbf{w}^0)]}{a_3^2 s_{4'}^2 (a_5^2 + a_6^2) + [a_5 (a_2 + a_4) - a_3 a_6 c_{4'}]^2}, \\ {}^0\mathbf{z}_4^0 = \frac{{}^0\mathbf{w}^0 - {}^0\mathbf{e}^0 - a_5 {}^0\mathbf{x}_4^0}{a_6}, \\ {}^0\mathbf{y}_4^0 = {}^0\mathbf{z}_4^0 \times {}^0\mathbf{x}_4^0 = \frac{a_3 c_{4'} {}^0\mathbf{x}_4^0 + (a_2 + a_4) {}^0\mathbf{z}_4^0 - {}^0\mathbf{e}^0}{a_3 s_{4'}}. \end{cases} \quad (32)$$

Therefore, the initial attitude matrix is

$${}^0\mathbf{R}_4^{\psi=0} = [{}^0\mathbf{x}_4^0 \quad {}^0\mathbf{y}_4^0 \quad {}^0\mathbf{z}_4^0]. \quad (33)$$

From the definition of  ${}^0\mathbf{R}_\psi$ , we obtain

$${}^0\mathbf{R}_\psi = \mathbf{I}_3 + [\mathbf{u}_w \times] \sin \psi + [\mathbf{u}_w \times]^2 (1 - \cos \psi), \quad (34)$$

where  $[\mathbf{u}_w \times]$  denotes the skew-symmetric matrix of vector  $\mathbf{w}$ .

In summary,  ${}^0\mathbf{R}_4$  can be solved by Eq. (24).

### 3.2.3 Analytical solution of $\theta'_1$ , $\theta'_2$ , and $\theta'_3$

Joint angle  $\theta'_4$  of the SRS manipulator has been solved, so  ${}^3\mathbf{R}_4$  is a known quantity.

On the one hand,  ${}^0\mathbf{R}_3$  can be obtained as follows:

$$\begin{aligned} {}^0\mathbf{R}_3 &= {}^0\mathbf{R}_4 {}^3\mathbf{R}_4^{-1} = {}^0\mathbf{R}_\psi {}^0\mathbf{R}_4^{\psi=0} {}^3\mathbf{R}_4^{-1} \\ &= \begin{bmatrix} a_{s11} & a_{s12} & a_{s13} \\ a_{s21} & a_{s22} & a_{s23} \\ a_{s31} & a_{s32} & a_{s33} \end{bmatrix}, \end{aligned} \quad (35)$$

where  $a_{sij}$  ( $i, j = 1, 2, 3$ ) represent the element of the  $i$ th row and  $j$ th column of matrix  ${}^0\mathbf{R}_3$ .

On the other hand, in accordance with forward kinematics,

$$\begin{aligned} {}^0\mathbf{R}_3 &= {}^0\mathbf{R}_{0'} {}^0\mathbf{R}_1 {}^1\mathbf{R}_2 {}^2\mathbf{R}_3 \\ &= \begin{bmatrix} -s_2' s_3' & -s_2' c_3' & -c_2' \\ -s_1' c_3' - c_1' c_2' s_3' & s_1' s_3' - c_1' c_2' c_3' & c_1' s_2' \\ s_1' c_2' s_3' - c_1' c_3' & c_1' s_3' + s_1' c_2' c_3' & -s_1' s_2' \end{bmatrix}. \end{aligned} \quad (36)$$

Equations (35) and (36) are equal, and  $\theta'_1$ ,  $\theta'_2$ , and  $\theta'_3$  can be solved as follows:

$$\theta'_2 = \pm \arccos(-a_{s13}), \quad (37)$$

$$\theta'_1 = \arctan 2(-a_{s33} s_2', a_{s23} s_2'), \quad (38)$$

$$\theta'_3 = \arctan2(-a_{s11}s_{2'}, -a_{s12}s_{2'}). \quad (39)$$

### 3.2.4 Analytical solution of $\theta'_5$ , $\theta'_6$ , and $\theta'_7$

On the one hand,  ${}^{\text{EE}}\mathbf{R}_4$  can be obtained as follows:

$$\begin{aligned} {}^{\text{EE}}\mathbf{R}_4 &= {}^0\mathbf{R}_{\text{EE}}^{-10} \mathbf{R}_4 = {}^0\mathbf{R}_{\text{EE}}^{-10} \mathbf{R}_{\psi}^0 \mathbf{R}_4^{\psi=0} \\ &= \begin{bmatrix} a_{w11} & a_{w12} & a_{w13} \\ a_{w21} & a_{w22} & a_{w23} \\ a_{w31} & a_{w32} & a_{w33} \end{bmatrix}, \end{aligned} \quad (40)$$

where  $a_{wij}$  ( $i, j = 1, 2, 3$ ) represent the element of the  $i$ th row and  $j$ th column of matrix  ${}^{\text{EE}}\mathbf{R}_4$ .

On the other hand, in accordance with forward kinematics,

$$\begin{aligned} {}^{\text{EE}}\mathbf{R}_4 &= ({}^4\mathbf{R}_5 {}^5\mathbf{R}_6 {}^6\mathbf{R}_7 {}^{\text{EE}}\mathbf{R}_{\text{EE}})^{-1} \\ &= \begin{bmatrix} s_{5'}s_{6'} & -c_{5'}s_{6'} & c_{6'} \\ c_{5'}s_{7'} + s_{5'}c_{6'}c_{7'} & s_{5'}s_{7'} - c_{5'}c_{6'}c_{7'} & -s_{6'}c_{7'} \\ c_{5'}c_{7'} - s_{5'}c_{6'}s_{7'} & s_{5'}c_{7'} + c_{5'}c_{6'}s_{7'} & s_{6'}s_{7'} \end{bmatrix}. \end{aligned} \quad (41)$$

Equations (40) and (41) are equal, and  $\theta'_5$ ,  $\theta'_6$ , and  $\theta'_7$  can be solved as follows:

$$\theta'_6 = \pm \arccos a_{w13}, \quad (42)$$

$$\theta'_5 = \arctan2(a_{w11}s_{6'}, -a_{w12}s_{6'}), \quad (43)$$

$$\theta'_7 = \arctan2(a_{w33}s_{6'}, -a_{w23}s_{6'}). \quad (44)$$

## 3.3 Approximate analytical solution of the EMM based on arm angle parameterization

### 3.3.1 Relationship of joint angles between the EMM and the SRS manipulator

The difference between the EMM and the SRS manipulator is that offset  $a_1$  and  $a_7$  of the shoulder and wrist are not zero. In accordance with the solutions of the EMM based on joint angle parameterization in Section 2.2, we can obtain the relationship of joint angles between the EMM and the SRS manipulator, as shown in Table 2. With the same  ${}^0\mathbf{T}_{\text{EE}}$ , joint angles  $\theta_1$ ,  $\theta_2$ ,  $\theta_6$ , and  $\theta_7$  of the two types of manipulators are the same, but  $\theta_3$ ,  $\theta_4$ , and  $\theta_5$  are different.  $\theta_3 + \theta_4 + \theta_5$  is also the same.

### 3.3.2 Approximate analytical solution of each joint angle

In accordance with the analysis in Table 2 and the solutions of the SRS manipulator based on arm angle parameterization in Section 3.2, the analytical inverse kinematic

solution of the EMM based on arm angle parameterization can be obtained as follows:

$$\theta_1 = \arctan2(-a_{s33}s_{2'}, a_{s23}s_{2'}), \quad (45)$$

$$\theta_2 = \pm \arccos(-a_{s13}), \quad (46)$$

$$\theta_6 = \pm \arccos a_{w13}, \quad (47)$$

$$\theta_7 = \arctan2(a_{w33}s_{6'}, -a_{w23}s_{6'}), \quad (48)$$

$$\theta_4 = \pm \arccos \frac{A^2 + B^2 - a_3^2 - a_5^2}{2a_3a_5}, \quad (49)$$

$$\theta_3 = \arctan2[A(a_3 + a_5c_4) - Ba_5s_4, B(a_3 + a_5c_4) + Aa_5s_4], \quad (50)$$

$$\begin{aligned} \theta_5 &= (\theta_3 + \theta_4 + \theta_5) - (\theta_3 + \theta_4) \\ &= \arctan2(s_{345}, c_{345}) - (\theta_3 + \theta_4). \end{aligned} \quad (51)$$

The expressions of related parameters are shown in Table 2. The symbol of  $\theta_4$  must be consistent with that of  $\theta'_4$ .

Given the value of arm angle  $\psi$ , eight solutions of the EMM can be solved based on arm angle parameterization.  $\theta_3$ ,  $\theta_4$ , and  $\theta_5$  calculated by these formulas are different because the offsets of the two manipulators are different. Therefore, the actual arm angles corresponding to the eight solutions are not the given  $\psi$ . These errors are uncontrollable.

We define the given  $\psi$  as the nominal arm angle, and  $\tilde{\psi}$  corresponding to the solution calculated by  $\psi$  is called the actual arm angle.

### 3.3.3 Case analysis

The position and attitude of the end-effector are given as follows:

$${}^0\mathbf{T}_{\text{EE}} = \begin{bmatrix} -0.7389 & -0.3815 & -0.5554 & 1.4348 \\ 0.3300 & -0.9236 & 0.1953 & 1.9698 \\ -0.5875 & -0.0390 & 0.8083 & 1.0302 \\ 0 & 0 & 0 & 1 \end{bmatrix}. \quad (52)$$

Given nominal arm angle  $\psi = 135^\circ$ , eight solutions of the EMM can be solved in accordance with Section 3.3.2, and actual arm angle  $\tilde{\psi}$  corresponding to each solution can be calculated in accordance with Section 3.1, as shown in Table 3.

The actual arm angles calculated by eight solutions have errors. The maximum actual arm angle error is  $9.6177^\circ$ ,

**Table 2** Relationship of joint angles between the experimental module manipulator (EMM) and the spherical-roll-spherical (SRS) manipulator

Joint angle	EMM	SRS manipulator	Relationship
$\theta_1, \theta_2$	$(a_0 + p_x - a_8 n_x) c_2$ $+ [(a_8 n_y - p_y) c_1 + (p_z - a_8 n_z) s_1] s_2$ $+(a_2 + a_4 + a_6) = 0$	$(a_0 + p_x - a_8 n_x) c_{2'}$ $+ [(a_8 n_y - p_y) c_{1'} + (p_z - a_8 n_z) s_{1'}] s_{2'}$ $+(a_2 + a_4 + a_6) = 0$	$\theta_1 = \theta'_1, \theta_2 = \theta'_2$
$\theta_6$	$c_6 = -(n_z s_1 - n_y c_1) s_2 - n_x c_2$	$c_{6'} = -(n_z s_{1'} - n_y c_{1'}) s_{2'} - n_x c_{2'}$	$\theta_6 = \theta'_6$
$\theta_7$	$\begin{cases} c_7 = \frac{(s_z s_1 - s_y c_1) s_2 + s_x c_2}{s_6} \\ s_7 = -\frac{(a_z s_1 - a_y c_1) s_2 + a_x c_2}{s_6} \end{cases}$	$\begin{cases} c_{7'} = \frac{(s_z s_{1'} - s_y c_{1'}) s_{2'} + s_x c_{2'}}{s_{6'}} \\ s_{7'} = -\frac{(a_z s_{1'} - a_y c_{1'}) s_{2'} + a_x c_{2'}}{s_{6'}} \end{cases}$	$\theta_7 = \theta'_7$
$\theta_4$	$c_4 = \frac{A^2 + B^2 - a_3^2 - a_5^2}{2a_3 a_5}$	$c_{4'} = \frac{A'^2 + B'^2 - a_3'^2 - a_5'^2}{2a_3 a_5}$	The EMM $a_1 \neq 0$ and $a_7 \neq 0$ , and the SRS manipulator $a_1 = a_7 = 0$ . Therefore, $A \neq A'$ , $B \neq B'$ , $\theta_4 \neq \theta'_4$ , $\theta_3 \neq \theta'_3$ , and $\theta_5 \neq \theta'_5$ . $\theta_{345}$ has no relationship with $a_1$ and $a_7$ ; hence, $\theta_{345} = \theta_{3'4'5'}$ .
$\theta_3$	$\begin{cases} s_3 = \frac{A(a_3 + a_5 c_4) - B a_5 s_4}{a_3^2 + a_5^2 + 2a_3 a_5 c_4} \\ c_3 = \frac{B(a_3 + a_5 c_4) + A a_5 s_4}{a_3^2 + a_5^2 + 2a_3 a_5 c_4} \end{cases}$	$\begin{cases} s_{3'} = \frac{A'(a_3 + a_5 c_{4'}) - B' a_5 s_{4'}}{a_3^2 + a_5^2 + 2a_3 a_5 c_{4'}} \\ c_{3'} = \frac{B'(a_3 + a_5 c_{4'}) + A' a_5 s_{4'}}{a_3^2 + a_5^2 + 2a_3 a_5 c_{4'}} \end{cases}$	
$\theta_5$	$\theta_5 = (\theta_3 + \theta_4 + \theta_5) - (\theta_3 + \theta_4)$ $= \arctan2(s_{345}, c_{345}) - (\theta_3 + \theta_4)$	$\theta_{5'} = (\theta_{3'} + \theta_{4'} + \theta_{5'}) - (\theta_{3'} + \theta_{4'})$ $= \arctan2(s_{3'4'5'}, c_{3'4'5'}) - (\theta_{3'} + \theta_{4'})$	
$\theta_3 + \theta_4 + \theta_5$	$\begin{cases} s_{345} = -\frac{n_z c_1 + n_y s_1}{s_6} \\ c_{345} = -[(s_z c_1 + s_y s_1) s_7 \\ + (a_z c_1 + a_y s_1) c_7] \end{cases}$	$\begin{cases} s_{3'4'5'} = -\frac{n_z c_{1'} + n_y s_{1'}}{s_{6'}} \\ c_{3'4'5'} = -[(s_z c_{1'} + s_y s_{1'}) s_{7'} \\ + (a_z c_{1'} + a_y s_{1'}) c_{7'}] \end{cases}$	

Note:  $A = a_7[c_7((a_y c_1 - a_z s_1) c_2 + a_x s_2) + s_7((s_y c_1 - s_z s_1) c_2 + s_x s_2)] + a_8[(n_y c_1 - n_z s_1) c_2 + n_x s_2] + (p_z s_1 - p_y c_1) c_2 - (p_x + a_0) s_2$ ,  $B = -a_1 + a_7[(a_y s_1 + a_z c_1) c_7 + (s_y s_1 + s_z c_1) s_7] + a_8[(n_y s_1 + n_z c_1) - p_y s_1 - p_z c_1]$ ;  $A' = a_8[(n_y c_{1'} - n_z s_{1'}) c_{2'} + n_x s_{2'}] + (p_z s_{1'} - p_y c_{1'}) c_{2'} - (p_x + a_0) s_{2'}$ ,  $B' = a_8[(n_y s_{1'} + n_z c_{1'}) - p_y s_{1'} - p_z c_{1'}]$ .

and its relative error is up to 7.12%. This error cannot be ignored when precise control is required. Therefore, for the approximate inverse solution of the EMM based on arm angle parameterization, we need to correct actual arm angle  $\tilde{\psi}$  in reference to nominal arm angle  $\psi$ . Then, we can calculate eight precise inverse solutions.

## 4 Precise semi-analytical solution based on arm angle parameterization

### 4.1 Solution process

We propose a numerical method to correct the solution errors of the EMM based on arm angle parameterization in

Section 3 so that actual arm angle  $\tilde{\psi}$  is infinitely close to nominal arm angle  $\psi$ . Eight precise solutions can be solved by this method. The algorithm flowchart is shown in Fig. 4.

The analytical inverse kinematic solution is solved based on joint angle parameterization in Section 2.2. Given an arbitrary value of  $\theta_1$ , we can calculate the values of  $\theta_2$ ,  $\theta_3$ , ...,  $\theta_7$ . Thus,  $\theta_2$ ,  $\theta_3$ , ...,  $\theta_7$  are all functions of  $\theta_1$ .

$$\theta_j = f(\theta_1), j = 2, 3, \dots, 7, \quad (53)$$

where  $f(\cdot)$  is a nonlinear mapping function of each joint angle  $\theta_j$  ( $j = 2, 3, \dots, 7$ ) corresponding to  $\theta_1$  in Section 2.2.

When the configuration of the manipulator is known, we can calculate actual arm angle  $\tilde{\psi}$  as

**Table 3** Eight approximate solutions calculated by nominal arm angle  $\psi = 135^\circ$  and their actual arm angle  $\tilde{\psi}$  in Case 1

Inverse solution	$\theta_1/(^\circ)$	$\theta_2/(^\circ)$	$\theta_3/(^\circ)$	$\theta_4/(^\circ)$	$\theta_5/(^\circ)$	$\theta_6/(^\circ)$	$\theta_7/(^\circ)$	Actual arm angle $\tilde{\psi}/(^\circ)$
1	-75.0144	77.9015	-35.0088	-67.7947	-106.9448	108.4550	78.4236	129.7819
2	-75.0144	77.9015	-32.9623	-93.9476	97.1616	-108.4550	-101.5764	130.1939
3	104.9856	-77.9015	145.4975	-44.7304	-130.5154	108.4550	78.4236	142.4985
4	104.9856	-77.9015	157.5737	-83.3832	76.0612	-108.4550	-101.5764	142.5272
5	65.0858	129.3636	-170.4417	76.7806	-83.3659	87.0906	-58.9323	126.6470
6	65.0858	129.3636	-160.6816	39.4032	124.2514	-87.0906	121.0677	125.3823
7	-114.9142	-129.3636	12.8840	96.8902	-106.8012	87.0906	-58.9323	140.8476
8	-114.9142	-129.3636	10.8205	75.3257	96.8267	-87.0906	121.0677	140.3597

$$\tilde{\psi} = g(\theta_1, \theta_2, \theta_3, \theta_4, \theta_5, \theta_6, \theta_7), \quad (54)$$

where  $g(\cdot)$  is a nonlinear mapping function with a known configuration for the manipulator.

When we correct the arm angle error of each solution, we retain the value of  $\theta_1$  for this solution. In accordance with the actual precision requirement, we select stride  $\Delta\theta$  of  $\theta_1$ . When  $\theta_1 \pm \Delta\theta$ , joint angles  $\theta_2, \theta_3, \dots, \theta_7$  and actual

arm angle  $\tilde{\psi}$  can be calculated. The formulas for  $\theta_2, \theta_4$ , and  $\theta_6$  depend on the symbols of the corresponding angles calculated by Eqs. (4) or (5), (8), and (6), respectively.  $\theta_3, \theta_5$ , and  $\theta_7$  are calculated by Eqs. (9), (12), and (7), respectively. The change trend of actual arm angle  $\tilde{\psi}$  is the trend that is close to or far from nominal arm angle  $\psi$  because actual arm angle  $\tilde{\psi}$  changes monotonously in a  $2\pi$  period of  $\theta_1$  (analysis in Section 4.2). By comparing the magnitude of  $|\tilde{\psi} - \psi|$  in two cases, the change trend of actual arm angle  $\tilde{\psi}$  close to  $\psi$  is selected. Through stride  $\Delta\theta$  of  $\theta_1$ , actual arm angle  $\tilde{\psi}$  is updated continuously. The value of termination condition  $\varepsilon$  is selected reasonably. When  $|\tilde{\psi} - \psi| < \varepsilon$ , the calculation stops. In other words,

$$\lim_{\Delta\theta \rightarrow 0} |\tilde{\psi} - \psi| = 0. \quad (55)$$

Then, actual arm angle  $\tilde{\psi}$  and  $\theta_1, \theta_2, \dots, \theta_7$  are recorded at this moment.  $\theta_1, \theta_2, \dots, \theta_7$  are the precise joint angles after the arm angle error correction. The errors of the eight solutions are corrected. Then, we obtain eight precise inverse kinematic solutions based on arm angle parameterization.

A summary of the approach is presented as follows:

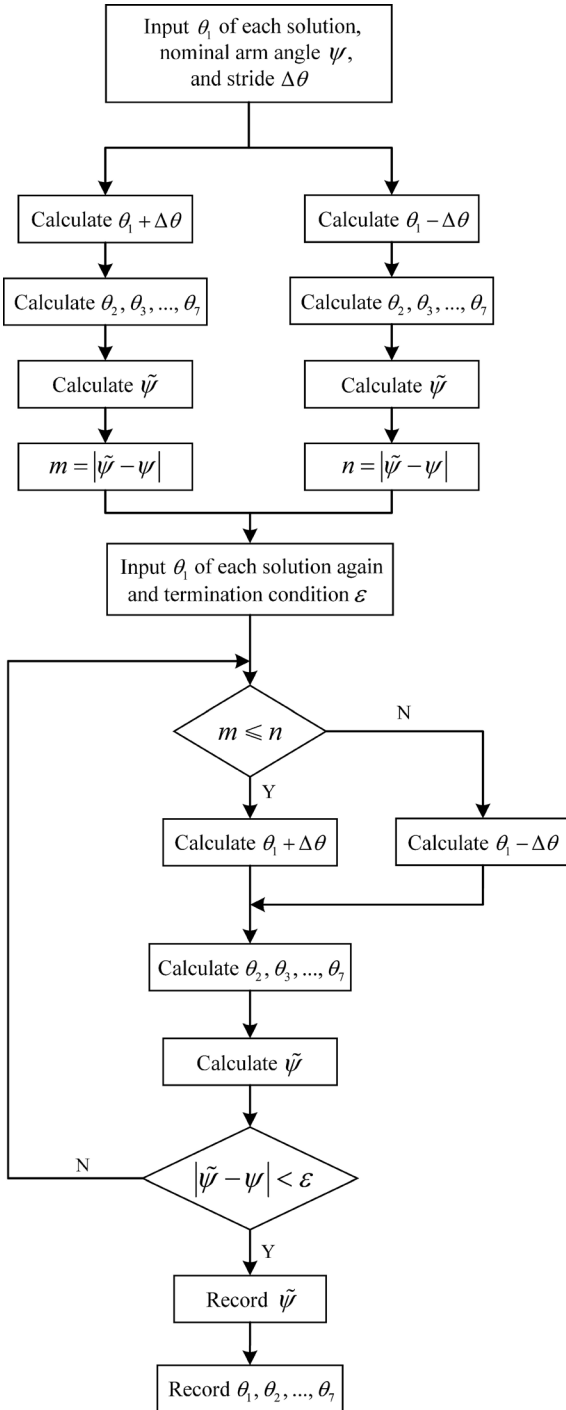
- Step 1: Given nominal arm angle  $\psi$ , select stride  $\Delta\theta$  and termination condition  $\varepsilon$  in accordance with the actual situation. Select joint angle  $\theta_1$  of each solution.
- Step 2: Calculate actual arm angle  $\tilde{\psi}$  when  $\theta_1 \pm \Delta\theta$ . Select the trend where  $\tilde{\psi}$  is close to  $\psi$ .
- Step 3: In accordance with this trend, calculate joint angles  $\theta_2, \theta_3, \dots, \theta_7$  and  $\tilde{\psi}$  through  $\theta_1$  and  $\Delta\theta$ .
- Step 4: Change the value of  $\theta_1$  through  $\Delta\theta$  and go to Step 3. Exit until  $\varepsilon$  reaches its precision.
- Step 5: Record  $\theta_1, \theta_2, \dots, \theta_7$ , and  $\tilde{\psi}$ .

#### 4.2 Case correction and analysis

Given stride  $\Delta\theta = 0.001^\circ$  and termination condition  $\varepsilon = 0.0006^\circ$ , eight approximate inverse kinematic solutions obtained by solving the case in Section 3.3.3 are corrected, as shown in Table 4. The manipulator configuration of the first precise solution is shown in Fig. 5.

The actual arm angle  $\tilde{\psi}$  of the eight solutions are all infinitely close to nominal arm angle  $\psi = 135^\circ$ . The maximum error is reduced from  $9.6177^\circ$  to  $0.0005^\circ$ . The minimum error is 0, which satisfies the actual precision requirement. The eight solutions are the precise inverse kinematic solutions of the EMM based on arm angle parameterization.

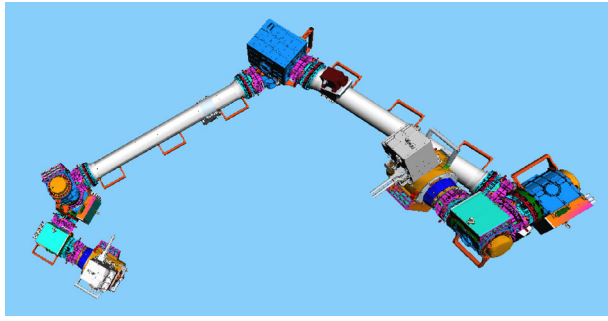
For analysis convenience,  $\theta_2$  calculated by Eqs. (4) and (5) are denoted as  $\theta_2^-$  and  $\theta_2^+$ , respectively. When  $\theta_4$  and  $\theta_6$  are calculated by Eqs. (8) and (6), the formulas of the positive values are denoted as  $\theta_4^+$  and  $\theta_6^+$ , and the formulas of the negative values are denoted as  $\theta_4^-$  and  $\theta_6^-$ . In Table 4, the curves for the actual arm angles  $\tilde{\psi}$  of the eight solutions corresponding to  $\theta_1 \in [-\pi, \pi]$  are shown in Fig. 6.



**Fig. 4** Flowchart for the algorithm for correcting the arm angle errors.

**Table 4** Eight precise solutions corrected to nominal arm angle  $\psi = 135^\circ$  and their actual arm angle  $\tilde{\psi}$  in Case 1

Inverse solution	$\theta_1/(\circ)$	$\theta_2/(\circ)$	$\theta_3/(\circ)$	$\theta_4/(\circ)$	$\theta_5/(\circ)$	$\theta_6/(\circ)$	$\theta_7/(\circ)$	Actual arm angle $\tilde{\psi}/(\circ)$
1	-79.6594	80.0057	-31.7645	-68.5655	-107.4127	112.4957	81.6077	134.9996
2	-79.2564	79.8118	-29.8156	-94.8141	96.7095	-112.1390	-98.6737	135.0003
3	111.1286	-75.5521	143.0353	-46.8091	-128.5043	103.3635	74.3511	135.0000
4	111.4466	-75.4437	154.0291	-84.2827	77.8483	-103.1072	-105.8565	134.9999
5	57.8508	124.0487	-170.7387	75.5782	-86.7634	81.7248	-53.1516	135.0002
6	56.9938	123.3800	-162.8315	40.3714	119.9489	-81.0841	127.5950	134.9995
7	-109.5662	-132.8739	14.2388	97.0154	-104.6965	90.9200	-62.6529	134.9997
8	-109.8352	-132.7062	12.9465	74.4857	98.9454	-90.7312	117.5244	135.0001


**Fig. 5** Experimental module manipulator configuration of the first precise solution in Case 1.

Regardless of which group of formulas is used for calculation, actual arm angle  $\tilde{\psi}$  changes monotonously in the interval  $[-\pi, \pi]$ . When we provide the value of nominal arm angle  $\psi$ ,  $\theta_1$  has only one solution. Therefore, only eight inverse kinematic solutions exist for the EMM based on arm angle parameterization. The method proposed in this section is effective.

## 5 Superiority of the arm angle parameterization method in parameter selection

In Section 2, we solve the inverse kinematics of the EMM based on joint angle parameterization. If we provide the homogeneous transformation matrix of the end-effector in the reachable operating space, several given  $\theta_1 \in [-\pi, \pi]$  cannot solve the other six joint angles. With  $\theta_2$  as an example, when  $\theta_2$  is calculated by Eqs. (4) and (5), the condition must be satisfied as follows:

$$-1 \leq \frac{-(a_2 + a_4 + a_6)}{\sqrt{a^2 + b^2}} \leq 1. \quad (56)$$

If  $\theta_1$  does not satisfy this condition, the manipulator will

be unsolvable. Therefore, the joint angle parameterization method has limitations on the given joint angle.

However, the arm angle parameterization method does not have these limitations on the given arm angle. In the case analysis in Section 3.3.3, given the homogeneous transformation matrix of the end-effector by Eq. (52), arbitrary  $\theta_1 \in [-\pi, \pi]$  can solve the other six joint angles. As shown in Fig. 6, arm angle  $\tilde{\psi}$  and joint angle  $\theta_1$  exhibit one-to-one correspondence in the interval  $[-\pi, \pi]$ .

When several given  $\theta_1 \in [-\pi, \pi]$  cannot solve the other six joint angles, we give the position and attitude of the end-effector as follows:

$${}^0T_{EE} = \begin{bmatrix} 0.5187 & 0.4184 & 0.7456 & -0.8786 \\ -0.6013 & -0.4415 & 0.6660 & 1.7019 \\ 0.6078 & -0.7938 & 0.0226 & 1.1783 \\ 0 & 0 & 0 & 1 \end{bmatrix}. \quad (57)$$

When the EMM has solutions, the range of  $\theta_1$  can be solved by Eq. (56) as follows:

$$\theta_1 \in [-180^\circ, -137.1457^\circ] \cup [-79.2755^\circ, 40.8543^\circ] \cup [100.7245^\circ, 180^\circ]. \quad (58)$$

Given nominal arm angle  $\psi = 135^\circ$ , eight approximate solutions can be solved in accordance with Section 3.3.2, as shown in Table 5. The actual arm angles calculated by the eight solutions have errors. The maximum actual arm angle error is  $12.2831^\circ$ , and its relative error is up to 9.10%. Given stride  $\Delta\theta = 0.001^\circ$  and termination condition  $\varepsilon = 0.002^\circ$ , the correction results in accordance with Section 4.1 are shown in Table 6. The maximum error of actual arm angle  $\tilde{\psi}$  is reduced from  $12.2831^\circ$  to  $0.0020^\circ$ . The minimum error is  $0.0004^\circ$ , which already satisfies the actual precision requirement. The manipulator configuration of the first precise solution is shown in Fig. 7.

The curves for the actual arm angles  $\tilde{\psi}$  of the eight

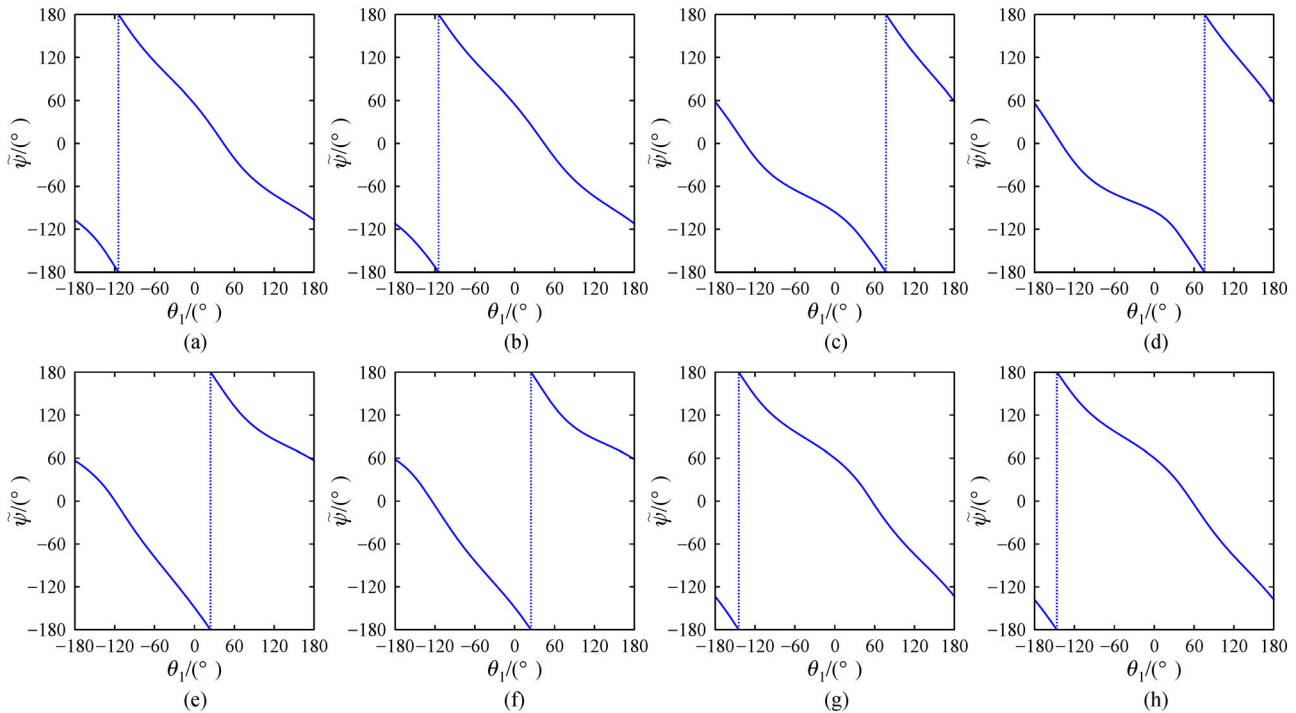


**Fig. 6** Curves of actual arm angles  $\tilde{\psi}$  correspond to  $\theta_1$  in Case 1: (a)  $\theta_2^+, \theta_4^-, \theta_6^+$ ; (b)  $\theta_2^+, \theta_4^-, \theta_6^-$ ; (c)  $\theta_2^-, \theta_4^-, \theta_6^+$ ; (d)  $\theta_2^-, \theta_4^-, \theta_6^-$ ; (e)  $\theta_2^+, \theta_4^+, \theta_6^+$ ; (f)  $\theta_2^+, \theta_4^+, \theta_6^-$ ; (g)  $\theta_2^-, \theta_4^+, \theta_6^+$ ; and (h)  $\theta_2^-, \theta_4^+, \theta_6^-$ .

**Table 5** Eight approximate solutions calculated by nominal arm angle  $\psi = 135^\circ$  and their actual arm angle  $\tilde{\psi}$  in Case 2

Inverse solution	$\theta_1/(^\circ)$	$\theta_2/(^\circ)$	$\theta_3/(^\circ)$	$\theta_4/(^\circ)$	$\theta_5/(^\circ)$	$\theta_6/(^\circ)$	$\theta_7/(^\circ)$	Actual arm angle $\tilde{\psi}/(^\circ)$
1	-74.5529	41.1411	59.0447	-147.0799	39.7875	96.3458	-25.6682	135.8676
2	-74.5529	41.1411	33.3418	-123.9961	-137.5933	-96.3458	154.3318	122.7169
3	105.4471	-41.1411	-127.4815	-121.8101	21.0440	96.3458	-25.6682	146.4159
4	105.4471	-41.1411	-151.1755	-97.6415	-159.4307	-96.3458	154.3318	136.0138
5	25.7588	113.7663	103.5857	97.3836	139.3401	121.8922	98.1554	138.8542
6	25.7588	113.7663	85.7979	125.7015	-51.1899	-121.8922	-81.8446	131.6935
7	-154.2412	-113.7663	-99.9945	121.7516	138.5523	121.8922	98.1554	139.3173
8	-154.2412	-113.7663	-124.9401	145.1176	-39.8680	-121.8922	-81.8446	125.0305

**Table 6** Eight precise solutions corrected to nominal arm angle  $\psi = 135^\circ$  and their actual arm angle  $\tilde{\psi}$  in Case 2

Inverse solution	$\theta_1/(^\circ)$	$\theta_2/(^\circ)$	$\theta_3/(^\circ)$	$\theta_4/(^\circ)$	$\theta_5/(^\circ)$	$\theta_6/(^\circ)$	$\theta_7/(^\circ)$	Actual arm angle $\tilde{\psi}/(^\circ)$
1	-74.2549	40.5634	58.1106	-147.0877	40.4691	96.8771	-25.9693	135.0011
2	-77.9949	51.0466	43.4482	-125.4135	-143.7159	-87.7922	159.8987	134.9980
3	113.0101	-31.4347	-137.9357	-123.3949	26.0090	105.8662	-30.5921	135.0012
4	105.9051	-40.2642	-151.8906	-97.6617	-159.0967	-97.1529	153.8738	135.0007
5	23.3078	116.7033	100.6682	97.9066	140.0811	118.3647	96.9436	135.0007
6	27.5818	111.2742	88.3354	125.4589	-52.2753	-124.7980	-80.9160	134.9985
7	-156.4982	-116.4861	-103.1285	121.4000	140.5163	118.6301	97.0378	135.0014
8	-150.2092	-107.8211	-117.2833	146.4267	-46.1905	-128.7216	-79.7563	135.0004

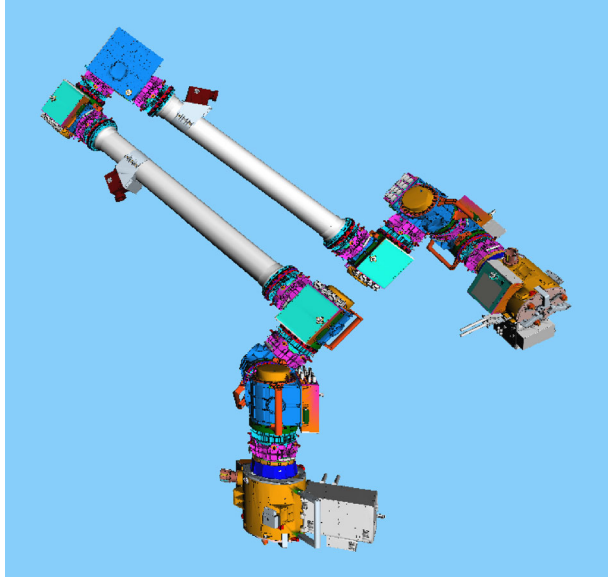


**Fig. 7** Experimental module manipulator of the first precise solution in Case 2.

solutions corresponding to  $\theta_1 \in [-\pi, \pi]$  are shown in Fig. 8. For this case, the change interval of  $\theta_1$  is not continuous. For the eight groups of formulas, the changes in actual arm angle  $\tilde{\psi}$  in the interval  $[-\pi, \pi]$  are shown in Table 7.

Therefore, for  $\tilde{\psi} \in [-\pi, \pi]$ , the arm angles  $\tilde{\psi}$  solved by

four groups of formulas have non-solution intervals and those solved by the four other groups of formulas have repetition-solution intervals.

When formulas  $\theta_4^-$  and  $\theta_6^+$  are used for calculation,  $\theta_2^+$  corresponds to the non-solution interval of  $\tilde{\psi}$ , and  $\theta_2^-$  corresponds to the repetition-solution interval of  $\tilde{\psi}$ . The ranges of the two intervals are the same. Therefore, when  $\tilde{\psi}$  takes an arbitrary value in the interval  $[-\pi, \pi]$ , although the change intervals of  $\tilde{\psi}$  are not continuous, two solutions can be solved after the two situations are combined. Similarly, we combine  $\theta_2^+$  and  $\theta_2^-$  corresponding to  $\theta_4^-$  and  $\theta_6^-$ ,  $\theta_4^+$  and  $\theta_6^+$ , and  $\theta_4^+$  and  $\theta_6^-$ . When  $\tilde{\psi}$  takes an arbitrary value in the interval  $[-\pi, \pi]$ , two solutions can also be solved for each situation. For the eight situations, we can solve the eight solutions of the EMM for arbitrary  $\tilde{\psi} \in [-\pi, \pi]$ .

In summary, when we provide the arbitrary position and attitude of the end-effector in the reachable operating space, several given  $\theta_1 \in [-\pi, \pi]$  cannot solve the EMM based on joint angle parameterization. However, arbitrary  $\tilde{\psi} \in [-\pi, \pi]$  can solve the EMM based on arm angle parameterization. That is, the arm angle parameterization method has great superiority over the joint angle parameterization method in parameter selection.

The approximate solutions are solved for the EMM based on arm angle parameterization in Section 3.3.3. The numerical correction method uses  $\theta_1$  of the approximate solutions as the initial calculation value. By selecting the appropriate stride  $\Delta\theta$ , we can solve the precise solutions

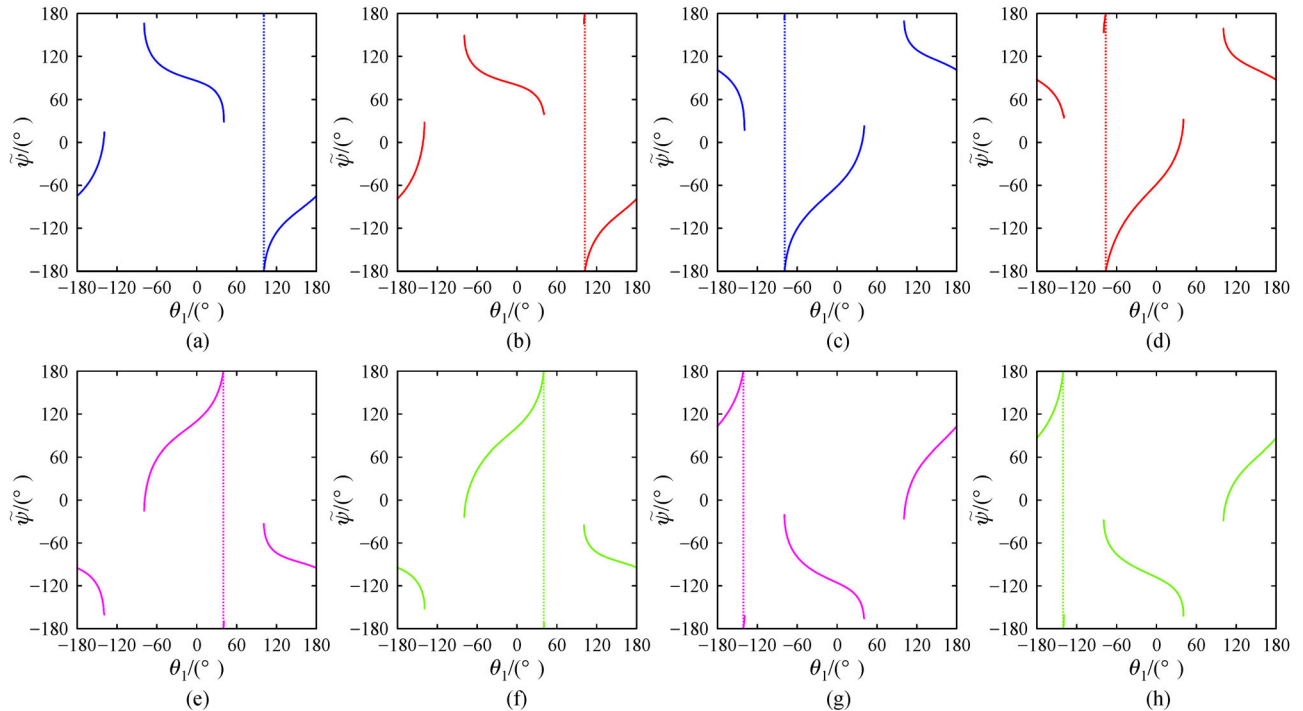


**Fig. 8** Curves of actual arm angles  $\tilde{\psi}$  correspond to  $\theta_1$  in Case 2: (a)  $\theta_2^+, \theta_4^-, \theta_6^+$ ; (b)  $\theta_2^+, \theta_4^-, \theta_6^-$ ; (c)  $\theta_2^-, \theta_4^-, \theta_6^+$ ; (d)  $\theta_2^-, \theta_4^-, \theta_6^-$ ; (e)  $\theta_2^-, \theta_4^+, \theta_6^+$ ; (f)  $\theta_2^-, \theta_4^+, \theta_6^-$ ; (g)  $\theta_2^+, \theta_4^+, \theta_6^+$ ; and (h)  $\theta_2^+, \theta_4^+, \theta_6^-$ .

**Table 7** Changes in actual arm angle  $\tilde{\psi}$  in the interval  $[-\pi, \pi]$ 

Combination of joint angles	Type of interval	Interval of actual arm angle $\tilde{\psi}/(^{\circ})$
$\theta_2^+, \theta_4^-, \theta_6^+$	Non-solution	$(16.1116, 26.2073) \cup (168.8087, 172.7647)$
$\theta_2^-, \theta_4^-, \theta_6^+$	Repetition-solution	$[16.1116, 26.2073] \cup [168.8087, 172.7647]$
$\theta_2^+, \theta_4^-, \theta_6^-$	Non-solution	$(31.4828, 36.0285) \cup (151.4337, 162.3077)$
$\theta_2^-, \theta_4^-, \theta_6^-$	Repetition-solution	$[31.4828, 36.0285] \cup [151.4337, 162.3077]$
$\theta_2^-, \theta_4^+, \theta_6^+$	Non-solution	$(-166.8049, -160.3144) \cup (-29.4358, -17.4838)$
$\theta_2^+, \theta_4^+, \theta_6^+$	Repetition-solution	$[-166.8049, -160.3144] \cup [-29.4358, -17.4838]$
$\theta_2^-, \theta_4^+, \theta_6^-$	Non-solution	$(-167.1600, -156.2214) \cup (-31.5175, -25.6658)$
$\theta_2^+, \theta_4^+, \theta_6^-$	Repetition-solution	$[-167.1600, -156.2214] \cup [-31.5175, -25.6658]$

quickly. If the initial value  $\theta_1$  of calculation is selected arbitrarily, for the situation where arbitrary  $\theta_1 \in [-\pi, \pi]$  can solve the other six joint angles, the amount of calculation will increase greatly although the precise solutions can be calculated by the correction method. The efficiency will be decreased greatly. For the situation where several given  $\theta_1 \in [-\pi, \pi]$  cannot solve the other six joint angles, the change intervals of  $\theta_1$  are not continuous. If the calculation reaches the end of an interval, it will be stopped, and the program will report errors. Therefore, the precise solutions cannot be calculated in this situation.

When stride  $\Delta\theta$  is too small, although the method has high precision, the amount of calculation increases greatly. In general, the higher the resolution we select, the lower the efficiency and the more optimal the solution we obtain. In accordance with the actual situation, we select stride  $\Delta\theta$  that not only satisfies the precision of calculation but also makes efficiency the highest.

## 6 Conclusions

This study proposes a high-precision, semi-analytical inverse method for 7-DOF redundant manipulators with link offset on the basis of arm angle parameterization. Previous studies could not solve precise inverse solutions by using arm angle parameterization because of the particularity of the configuration for the EMM, and the solutions that generalize the analytical results of the SRS manipulator to the EMM are approximate. In addition, the errors are uncontrollable. We propose a semi-analytical method and define the nominal and actual arm angles. The approximate solutions based on arm angle parameterization are corrected by the analytical solution based on joint angle parameterization. After selecting the stride and termination condition in accordance with the actual situation, the precise inverse solutions are calculated based on arm angle parameterization. The high precision of this method is verified by cases, and the minimum error approaches zero. The arm angle parameterization method has great superiority over the joint angle parameterization method in parameter selection.

## Nomenclature

### Abbreviations

CSSRMS	Chinese Space Station Remote Manipulator System
CMM	Core module manipulator
EMM	Experimental module manipulator
7-DOF	7-degree-of-freedom
SSRMS	Space Station Remote Manipulator System
SRS	Spherical-roll-spherical

### Variables

$a_i$ ( $i = 0, 1, \dots, 8$ )	Link length of the EMM
$a_{ij}$ ( $i, j = 1, 2, 3$ )	Element of the $i$ th row and $j$ th column of matrix ${}^0R_3$
$a_{wij}$ ( $i, j = 1, 2, 3$ )	Element of the $i$ th row and $j$ th column of matrix ${}^{EE}R_4$
$d$	Vector which is the projection of vector $e$ on vector $w$
$e$	Vector from shoulder point $S$ to elbow point $E$
${}^0e$	Vector expressed by $e$ in base coordinate system $\Sigma_0$
${}^0e^0$	Vector expressed by ${}^0e$ when arm angle $\psi = 0$
$I_3$	$3 \times 3$ identity matrix
$k$	Vector which is on the plane that contains vectors $V$ and $w$ and perpendicular to $w$
$\hat{k}$	Unit vector of $k$
$l$	Multiplication cross vector of $V$ and $w$ , defined as $l = V \times w$
$p$	Vector which is perpendicular to $w$ and passes through point $E$ , defined as $p = e - d$
$\hat{p}$	Unit vector of $p$
${}^0P_{EE}$	Position vector of end coordinate system $\Sigma_{EE}$ in base coordinate system $\Sigma_0$

${}^jR_i$ ( $i, j = 0, 1, \dots, 7, EE$ )	Rotation matrix of coordinate system $\Sigma_i$ relative to coordinate system $\Sigma_j$ (EE corresponds to end coordinate system $\Sigma_{EE}$ )
${}^0R_4^{\psi=0}$	Rotation matrix of coordinate system $\Sigma_4$ relative to base coordinate system $\Sigma_0$ when $\psi = 0$
${}^0R_\psi$	Rotation matrix which represents the rotation of arm angle $\psi$ about vector $\mathbf{w}$
${}^jT_i$ ( $i, j = 0, 1, \dots, 7, EE$ )	Homogeneous transformation matrix of coordinate system $\Sigma_i$ relative to coordinate system $\Sigma_j$
$[\mathbf{u}_l \times]$	Skew-symmetric matrix of vector $\mathbf{l}$
$[\mathbf{u}_w \times]$	Skew-symmetric matrix of vector $\mathbf{w}$
$\mathbf{V}$	Unit vector parallel to the rotation axis of joint 1
${}^0\mathbf{V}$	Vector expressed by $\mathbf{V}$ in base coordinate system $\Sigma_0$ , defined as ${}^0\mathbf{V} = [-1 \ 0 \ 0]^T$
$\mathbf{w}$	Vector from shoulder point $S$ to wrist point $W$
$\hat{\mathbf{w}}$	Unit vector of $\mathbf{w}$
${}^0\mathbf{w}$	Vector expressed by $\mathbf{w}$ in base coordinate system $\Sigma_0$
${}^0\mathbf{w}^0$	Vector expressed by ${}^0\mathbf{w}$ when arm angle $\psi = 0$
${}^4\mathbf{x}_3, {}^4\mathbf{y}_3, \text{ and } {}^4\mathbf{z}_3$	Unit vectors of three coordinate axes of coordinate system $\Sigma_3$ relative to coordinate system $\Sigma_4$
${}^0\mathbf{x}_4^0, {}^0\mathbf{y}_4^0, \text{ and } {}^0\mathbf{z}_4^0$	Unit vectors of three coordinate axes of coordinate system $\Sigma_4$ relative to base coordinate system $\Sigma_0$ when arm angle $\psi = 0$ , and ${}^0\mathbf{x}_3^0$ has the same meaning
$\alpha$	Angle from ${}^0\mathbf{w}^0$ rotation to ${}^0\mathbf{e}^0$
$\beta$	Angle between $SE_\perp$ and $E_\perp W_\perp$
$\psi$	Nominal arm angle of the EMM
$\tilde{\psi}$	Actual arm angle of the EMM
$\theta_i$ ( $i = 1, 2, \dots, 7$ )	Joint angle of the EMM
$\theta'_i$ ( $i = 1, 2, \dots, 7$ )	Joint angle of the SRS manipulator
$\theta_2^-$ and $\theta_2^+$	$\theta_2$ calculated by Eqs. (4) and (5)
$\theta_4^-$ and $\theta_4^+$	Formulas of the negative and positive values in accordance with $\theta_4$ calculated by Eq. (8)
$\theta_6^-$ and $\theta_6^+$	Formulas of the negative and positive values in accordance with $\theta_6$ calculated by Eq. (6)
$\Delta\theta$	Stride of $\theta_1$
$\varepsilon$	Iteration termination condition
$\Sigma_i$ ( $i = 0, 1, \dots, 7, EE$ )	Coordinate system of the manipulator

**Acknowledgements** This work was supported by the Foundation for Innovative Research Groups of the National Natural Science Foundation of China (Grant No. 51521003) and the Major Research Plan of National

Natural Science Foundation of China (Grant No. 91848202).

**Open Access** This article is licensed under a Creative Commons Attribution 4.0 International License, which permits use, sharing, adaptation, distribution, and reproduction in any medium or format as long as appropriate credit is given to the original author(s) and source, a link to the Creative Commons license is provided, and the changes made are indicated.

The images or other third-party material in this article are included in the article's Creative Commons license, unless indicated otherwise in a credit line to the material. If material is not included in the article's Creative Commons license and your intended use is not permitted by statutory regulation or exceeds the permitted use, you will need to obtain permission directly from the copyright holder.

To view a copy of this license, visit <http://creativecommons.org/licenses/by/4.0/>.

## References

- Yoshimitsu R, Yuguchi Y, Kobayashi A, et al. Dynamic simulator for HTV capture with Space Station Remote Manipulator System. In: Proceedings of the 12th International Symposium on Artificial Intelligence, Robotics and Automation in Space. Montreal: CSA, 2014, 1–8
- Rembala R, Ower C. Robotic assembly and maintenance of future space stations based on the ISS mission operations experience. *Acta Astronautica*, 2009, 65(7–8): 912–920
- Flores-Abad A, Ma O, Pham K, et al. A review of space robotics technologies for on-orbit servicing. *Progress in Aerospace Sciences*, 2014, 68: 1–26
- Sabatini M, Gasbarri P, Monti R, et al. Vibration control of a flexible space manipulator during on orbit operations. *Acta Astronautica*, 2012, 73(4–5): 109–121
- Nokleby S B. Singularity analysis of the Canadarm2. *Mechanism and Machine Theory*, 2007, 42(4): 442–454
- Coleshill E, Oshinowo L, Rembala R, et al. Dextre: Improving maintenance operations on the International Space Station. *Acta Astronautica*, 2009, 64(9–10): 869–874
- Boumans R, Heemskerk C. The European robotic arm for the international space station. *Robotics and Autonomous Systems*, 1998, 23(1–2): 17–27
- Krukewich K, Sexton J, Cavin K, et al. The systems engineering approach to the integration of the Space Station Remote Manipulator System on the International Space Station (ISS). *Space Technology* (Oxford, England), 1996, 16(1): 31–48
- Li D, Rao W, Hu C, et al. Overview of the Chinese Space Station manipulator. In: Proceedings of AIAA SPACE 2015 Conference and Exposition. Pasadena: AIAA, 2015, 1–6
- Liu H, Li Z, Liu Y, et al. Key technologies of TianGong-2 robotic hand and its on-orbit experiments. *SCIENTIA SINICA Technologica*, 2018, 48(12): 1313–1320 (in Chinese)
- Diffler M A, Mehling J S, Abdallah M E, et al. Robonaut 2—The first humanoid robot in space. In: Proceedings of the IEEE International Conference on Robotics and Automation. Shanghai: IEEE, 2011, 2178–2183
- Fukazu Y, Hara N, Kanamiya Y, et al. Reactionless resolved acceleration control with vibration suppression capability for JEMRMS/SFA. In: Proceedings of the IEEE International Conference

- on Robotics and Biomimetics. Bangkok: IEEE, 2009, 1359–1364
13. Imaida T, Yokokohji Y, Doi T, et al. Ground-space bilateral teleoperation of ETS-VII robot arm by direct bilateral coupling under 7-s time delay condition. *IEEE Transactions on Robotics and Automation*, 2004, 20(3): 499–511
14. Liu H, Jiang Z, Liu Y. Review of space manipulator technology. *Manned Spaceflight*, 2015, 21(5): 435–443 (in Chinese)
15. Baillieul J. Avoiding obstacles and resolving kinematic redundancy. In: *Proceedings of the IEEE International Conference on Robotics and Automation*. San Francisco: IEEE, 1986, 1698–1704
16. Guo D, Zhang Y. Acceleration-level inequality-based MAN scheme for obstacle avoidance of redundant robot manipulators. *IEEE Transactions on Industrial Electronics*, 2014, 61(12): 6903–6914
17. Stevenson R, Shirinzadeh B, Alici G. Singularity avoidance and aspect maintenance in redundant manipulators. In: *Proceedings of the 7th International Conference on Control, Automation, Robotics and Vision*. Singapore: IEEE, 2002, 857–862
18. Xu W, Zhang J, Liang B, et al. Singularity analysis and avoidance for robot manipulators with nonspherical wrists. *IEEE Transactions on Industrial Electronics*, 2016, 63(1): 277–290
19. Hollerbach J M, Suh K C. Redundancy resolution of manipulators through torque optimization. In: *Proceedings of the IEEE International Conference on Robotics and Automation*. St. Louis: IEEE, 1985, 1016–1021
20. Zhang Y, Li W, Yu X, et al. Encoder based online motion planning and feedback control of redundant manipulators. *Control Engineering Practice*, 2013, 21(10): 1277–1289
21. Groom K N, Maciejewski A A, Balakrishnan V. Real-time failure-tolerant control of kinematically redundant manipulators. *IEEE Transactions on Robotics and Automation*, 1999, 15(6): 1109–1115
22. Jamisola R S, Maciejewski A A, Roberts R G. Failure-tolerant path planning for kinematically redundant manipulators anticipating locked-joint failures. *IEEE Transactions on Robotics*, 2006, 22(4): 603–612
23. She Y, Xu W, Su H, et al. Fault-tolerant analysis and control of SSRMS-type manipulators with single-joint failure. *Acta Astronautica*, 2016, 120: 270–286
24. Singh G K, Claassens J. An analytical solution for the inverse kinematics of a redundant 7DoF manipulator with link offsets. In: *Proceedings of the IEEE/RSJ International Conference on Intelligent Robots and Systems*. Taipei: IEEE, 2010, 2976–2982
25. Seraji H. Configuration control of redundant manipulators: Theory and implementation. *IEEE Transactions on Robotics and Automation*, 1989, 5(4): 472–490
26. Dubey R V, Euler J A, Babcock S M. Real-time implementation of an optimization scheme for seven-degree-of-freedom redundant manipulators. *IEEE Transactions on Robotics and Automation*, 1991, 7(5): 579–588
27. Shah M, Patel R V. Inverse Jacobian based hybrid impedance control of redundant manipulators. In: *Proceedings of the IEEE International Conference Mechatronics and Automation*. Niagara Falls: IEEE, 2005, 55–60
28. Colomé A, Torras C. Closed-loop inverse kinematics for redundant robots: Comparative assessment and two enhancements. *IEEE/ASME Transactions on Mechatronics*, 2015, 20(2): 944–955
29. Lee S, Bejczy A K. Redundant arm kinematic control based on parameterization. In: *Proceedings of the IEEE International Conference on Robotics and Automation*. Sacramento: IEEE, 1991, 458–465
30. Zu D, Wu Z, Tan D. Efficient inverse kinematic solution for redundant manipulators. *Chinese Journal of Mechanical Engineering*, 2005, 41(6): 71–75 (in Chinese)
31. Kreutz-Delgado K, Long M, Seraji H. Kinematic analysis of 7-DOF manipulators. *International Journal of Robotics Research*, 1992, 11(5): 469–481
32. Shimizu M, Kakuya H, Yoon W K, et al. Analytical inverse kinematic computation for 7-DOF redundant manipulators with joint limits and its application to redundancy resolution. *IEEE Transactions on Robotics*, 2008, 24(5): 1131–1142
33. Xu W, Yan L, Mu Z, et al. Dual arm-angle parameterisation and its applications for analytical inverse kinematics of redundant manipulators. *Robotica*, 2016, 34(12): 2669–2688
34. Zhou D, Ji L, Zhang Q, et al. Practical analytical inverse kinematic approach for 7-DOF space manipulators with joint and attitude limits. *Intelligent Service Robotics*, 2015, 8(4): 215–224
35. Dereli S, Koker R. Calculation of the inverse kinematics solution of the 7-DOF redundant robot manipulator by the firefly algorithm and statistical analysis of the results in terms of speed and accuracy. *Inverse Problems in Science and Engineering*, 2020, 28(5): 601–613
36. Faroni M, Beschi M, Pedrocchi N. Inverse kinematics of redundant manipulators with dynamic bounds on joint movements. *IEEE Robotics and Automation Letters*, 2020, 5(4): 6435–6442
37. Gong M, Li X, Zhang L. Analytical inverse kinematics and self-motion application for 7-DOF redundant manipulator. *IEEE Access: Practical Innovations, Open Solutions*, 2019, 7: 18662–18674
38. Kelemen M, Virgala I, Liptak T, et al. A novel approach for a inverse kinematics solution of a redundant manipulator. *Applied Sciences*, 2018, 8(11): 2229
39. Crane C D III, Duffy J, Carnahan T. A kinematic analysis of the space station remote manipulator system (SSRMS). *Journal of Robotic Systems*, 1991, 8(5): 637–658
40. Yu C, Jin M, Liu H. An analytical solution for inverse kinematic of 7-DOF redundant manipulators with offset-wrist. In: *Proceedings of the IEEE International Conference on Mechatronics and Automation*. Chengdu: IEEE, 2012, 92–97
41. Abbasi V, Azria B, Tabarah E, et al. Improved 7-DOF control of ISS robotic manipulators. In: *Proceedings of AIAA Space OPS 2004 Conference*. Montreal: AIAA, 2004
42. Lu S, Gu Y, Zhao J, et al. An iterative calculation method for solve the inverse kinematics of a 7-DOF robot with link offset. In: Huang Y, Wu H, Liu H, et al., eds. *Intelligent Robotics and Applications. ICIRA 2017. Lecture Notes in Computer Science*, vol 10464. Cham: Springer
43. Jin M, Liu Q, Wang B, et al. An efficient and accurate inverse kinematics for 7-DOF redundant manipulators based on a hybrid of analytical and numerical method. *IEEE Access: Practical Innovations, Open Solutions*, 2020, 8: 16316–16330
44. Xu W, Zhang J, Yan L, et al. Parameterized inverse kinematics resolution method for a redundant space manipulator with link offset. *Journal of Astronautics*, 2015, 36(1): 33–39 (in Chinese)
45. Craig J J. *Introduction to Robotics: Mechanics and Control*. 4th ed. New York: Pearson Education Inc., 2005